Composition dependence of interband transition intensities in GaPN, GaAsN, and GaPAs alloys

L. Bellaiche, Su-Huai Wei, and Alex Zunger
National Renewable Energy Laboratory, Golden, Colorado 80401
(Received 10 April 1997)

Using large (512-atom) pseudopotential supercell calculations, we have investigated the composition dependence of the momentum matrix element $M_{v,c}$ for transitions between the valence-band maximum and the conduction-band minimum of three semiconductor alloys: $GaP_{1-x}N_x$ and $GaAs_{1-x}N_x$, exhibiting large chemical and size differences between their alloyed elements, and $GaP_{1-x}As_x$, which is a weakly perturbed alloy. In the composition ranges where these alloys have a direct band gap, we find that (i) in $GaP_{1-x}As_x$, $M_{v,c}$ is large (like the virtual-crystal value) and nearly composition independent; (ii) in $GaAs_{1-x}N_x$, $M_{v,c}$ is strongly composition dependent: large for small x and small for large x; and (iii) in $GaP_{1-x}N_x$, $M_{v,c}$ is only slightly composition dependent and is significantly reduced relative to the virtual-crystal value. The different behavior of $GaP_{1-x}As_x$, $GaP_{1-x}N_x$, and $GaAs_{1-x}N_x$ is traced to the existence/absence of impurity levels at the dilute alloy limits: (a) there are no gap-level impurity states at the $x\rightarrow 1$ or $x\rightarrow 0$ limits of $GaP_{1-x}As_x$, (b) an isolated As impurity in GaN (GaN:As) has a deep band gap impurity level but no deep impurity state is found for N in GaAs, and (c) GaN:P exhibits a P-localized deep band-gap impurity state and GaP:N has an N-localized resonant state. The existence of deep levels leads to wave-function localization in real space, thus to a spectral spread in momentum space and to a reduction of $M_{v,c}$. These impurity levels are facilitated by atomic relaxations, as evident by the fact that unrelaxed GaN:As and GaN:P, show no deep levels, have extended wave functions, and have large interband transition elements. [S0163-1829(97)05339-3]

I. INTRODUCTION: WHY SHOULD THE INTERBAND TRANSITION INTENSITY IN ALLOYS DEPEND ON COMPOSITION?

Research on random substitutional $A_{1-x}B_x$ solid solutions often focuses on understanding the composition x dependence of various physical properties $P(x)$ such as phase diagrams,[1] mixing enthalpies and entropies,[1,2] band gaps of nonmetals,[3–6] density of states of metal[7,8] and nonmetal alloys,[5,6] and interatomic bond distances.[2,9,10] Little is known, however, about the composition dependence of the *intensity* of interband transitions, as reflected by the square of the momentum ($\mathbf{p}$) matrix element $M_{v,c}=|\langle v|\mathbf{p}|c\rangle|^2$ of valence $|v\rangle$ to conduction $|c\rangle$ excitations. The basic physics underlying this question is as follows: In a random $A_{1-x}B_x$ alloy whose lattice sites are occupied by the alloyed elements A and B with random probabilities $1-x$ and x, respectively, there are many crystallographically distinct A sites (and, separately, B sites) in that each A atom in the alloy could have locally a different number of A and B atoms as neighbors. Thus one could have in the random alloy a distribution of many different local chemical environments, even though the constituent ordered solids have but one or just a few repeated local chemical motifs (e.g., A_4 or B_4 tetrahedra). Depending on the chemical disparity between the atoms A and B and on their relative atomic sizes, atoms in the alloy will relax off their nominal lattice positions. Such relaxations could lead to a distribution of interatomic distances, on top of the distribution of local chemical environments. One can compute from a supercell approach to band theory various physical properties $P_\sigma(x)$ of this random alloy, including momentum matrix elements. How different will this momentum matrix element $P(x)$ be from the same property in the constituent, parent solids, or from the composition-weighted value $\overline{P(x)}=(1-x)P_A+xP_B$? To address this question, it is convenient to think[4] of the electronic wave functions $\psi_i(\overline{\mathbf{K}},\mathbf{r})$ of the alloy in the supercell representation (where $\overline{\mathbf{K}}$ is a wave vector in the small Brillouin zone, corresponding to the large real-space alloy supercell), as a linear combination of the wave functions $\phi_j(\mathbf{k},\mathbf{r})$ of the constituent solids:

$$\psi_i(\overline{\mathbf{K}},\mathbf{r})=\sum_{\mathbf{k}}\sum_{\mathbf{j}}\mathbf{B}_{ij}(\overline{\mathbf{K}},\mathbf{k})\,\phi_j(\mathbf{k},\mathbf{r}). \tag{1}$$

Here j is the band index and $\mathbf{k}$ is a wave vector in its Brillouin zone. For concreteness, $\phi_j(\mathbf{k},\mathbf{r})$ could be taken as the Bloch wave functions of a *virtual* $A_{1-x}B_x$ crystal, i.e., one with an average bond length $R(x)=(1-x)R_A+xR_B$ and an average potential $V(\mathbf{r},x)=(1-x)V_A(\mathbf{r})+xV_B(\mathbf{r})$. Like pure A or pure B, the virtual-crystal alloy (VCA) too lacks a distribution of local chemical environments or a distribution of bond lengths. (Note that the VCA is used here merely as a basis set, not as a physical approximation.) This discussion helps clarify the expected differences between the alloy eigenstates and interband transition and those of its constituents, in terms of two effects.

(i) Sublattice localization. While the existence of a unique, repeated local chemical motif in the periodic (A or B) parent systems and in the virtual alloy leads invariably to extended wave functions (so, for example, there are no separate ''A features'' and ''B features'' in the VCA spectrum), a real alloy could exhibit wave-function localization around particular sites within the supercell.

(ii) Interband mixing. An individual alloy state $\psi_i(\overline{\mathbf{K}},\mathbf{r})$ can have nonzero projection $B_{i,j}(\overline{\mathbf{K}},\mathbf{k})$ onto more than one VCA state. Thus the alloy state need not be a ''pure'' VCA state. For example, if the conduction-band minimum (CBM)

in the parent system is of X_{1c} symmetry, the transition to the Γ_v-type valence-band maximum (VBM) is dipole forbidden. But in the alloy supercell, the CBM could have a Γ_{1c} component so the transition to the VBM can be partially allowed. Such mixing does not exist in the pure parent solids.

Sublattice localization and interband mixing could alter the nature of alloy wave functions relative to the constituents. This could change the interband transition intensities relative to the constituents, leading to a ''bowing'' of the photoluminescence (PL) intensity.

Previous theoretical and experimental studies of the composition dependence of interband transition intensities are scant. In their supercell tight-binding calculation, Koiller and Capaz[11] find that the interband transition dipole matrix element of $Ga_{1-x}Al_xAs$ is nearly independent of the composition and almost equal to that of pure GaAs for all the compositions of the direct gaplike region. On the other hand, Yoshimoto *et al.*[12] show that the PL intensity of the near-band-edge emission of $Ga_{1-x}In_xN$ decreases considerably as the indium composition increases and Baillargeon *et al.*[13] found a decrease in the PL intensity of $GaP_{1-x}N_x$ as x increases (from 0.01 to 0.02). It is thus possible that the intensity of interband transitions depends on the chemical and size disparities between the constituents of the alloy [(Al,Ga) being similar, while (Ga,In) and (P,N) are more different].

In Refs. 14 and 15 we showed how localization in isovalent alloys leads to an anomalous composition-dependent and large *optical bowing coefficient*. Here we extend these studies to the compositional dependence of *interband transition intensities*. We conjecture that wave-function localization and the attendant irregular composition dependence of the optical bowing and the interband transition intensities will exist in those alloys where in the dilute (impurity) limit there are deep band-gap states. The following alloys could thus show these effects: CdSTe, ZnSTe, and GaPBi. To check this hypothesis, we study in this paper the composition dependence of the interband dipole matrix element between the VBM and CBM of three different isovalent semiconductor alloys of cubic (zinc-blende) constituents: ''strongly perturbed'' alloys $GaAs_{1-x}N_x$ and $GaP_{1-x}N_x$ exhibiting large chemical and size disparities between their constituents GaAs or GaP and GaN, versus a ''weakly perturbed'' alloy $GaP_{1-x}As_x$ exhibiting greater similarity between its constituents GaP and GaAs (see Table I and Refs. 14 and 16–19). Here only perfectly random, homogeneous alloys are treated. The effect of clustering on the electronic properties[20] is not discussed in the present study. Significant differences in the direct-gap momentum matrix element $M_{v,c}$ vs x dependence are found in these three alloys. (a) In the weakly perturbed $GaP_{1-x}As_x$ alloy, $M_{v,c}$ is nearly composition independent in the direct-band-gap region and similar in magnitude to the VCA value, indicating weak sublattice localization and interband mixing. On the other hand, (b) in the strongly perturbed $GaAs_{1-x}N_x$ alloy, $M_{v,c}$ depends strongly on composition: It is large for small x and small for large x. Finally, (c) in the direct-band-gap region of $GaP_{1-x}N_x$ alloys, $M_{v,c}$ depends slightly on composition and is significantly attenuated relative to the VCA value. The different behaviors of the three alloys originate from the existence/absence of impurity levels at the dilute alloy limits and its ensuing wave-function localizations: There are no deep, band-gap impurity states for GaAs:P and GaP:As. On the other hand, GaN:As has a deep band-gap level, leading to a strong VBM wave-function localization around As. Similarly, GaN:P exhibits a P-localized deep impurity state, while GaP:N has an N-localized resonant state. This localization is facilitated by significant atomic relaxation off the zinc-blende lattice sites and leads to a spectral spread in momentum space and to a far weaker transition intensity than expected from the pure Γ_{15v} VBM and Γ_{1c} CBM of the virtual lattice.

TABLE I. Comparison of some physical properties of bulk GaAs-GaN, GaP-GaN, and GaP-GaAs pairs and the corresponding anions. $\Delta a/a$ is the lattice mismatch and Δf is the difference in Phillips's electronegativities of the atoms on the mixed sublattice (Ref. 16). The differences of atomic s and p orbital energies $\Delta\epsilon_s$ and $\Delta\epsilon_p$, respectively, are calculated within the LDA approach using the Ceperley-Alder exchange and correlation (Ref. 17) as parametrized by Perdew and Zunger (Ref. 18). The unstrained band offset between GaP and GaAs, ΔE_v(GaP/GaAs), was fitted to the LDA value of Ref. 19. The valence-band offset between GaP and GaN, ΔE_v(GaP/GaN), was estimated by subtracting ΔE_v(GaP/GaAs) (+0.31 from Ref. 14) from ΔE_v(GaN/GaAs) (equal to +2.28 in Ref. 14). A negative value of $\Delta E_v(GaY/GaX)$ indicates that the VBM of GaX is lower than that of GaY.

Property	GaAs-GaN	GaP-GaN	GaP-GaAs
$\Delta a/a$ (%)	22.5	18.9	3.6
Δf	−1.43	−1.36	+0.07
$\Delta\epsilon_s$ (eV)	+3.72	+4.40	+0.68
$\Delta\epsilon_p$ (eV)	+1.90	+1.64	−0.26
ΔE_v (eV)	−2.28	−1.97	+0.31

II. METHOD OF CALCULATION

A large (512-atom) supercell representation is used for the alloys. For each composition, the alloyed elements are distributed at random on the fcc anion lattice sites, fully relaxing all atomic positions via a conjugate gradient minimization of a parametrized valence force field (VFF).[21,22] The lattice constant of the alloys is assumed here to vary linearly as a function of the composition x, as actually found for $GaAs_{1-x}N_x$ in first-principles local-density approximation (LDA) total-energy calculations.[15,23] We used in the VFF method the bond-stretching (α) and bond-bending (β) force constants of Ref. 24 for GaN ($\alpha=96.30$ N/m and $\beta=14.80$ N/m) and of Ref. 22 for GaAs ($\alpha=41.19$ N/m and $\beta=8.94$ N/m) and for GaP ($\alpha=47.32$ N/m and $\beta=10.44$ N/m). In a previous work (Table I in Ref. 14) we compared the calculated structural relaxation parameters of some *ordered* $GaAs_{1-x}N_x$ alloys using the VFF and using the first-principles linearized augmented plane-wave method[15], and found that the VFF follows the structural trends in the first-principles results reasonably well.

The electronic properties of the relaxed supercell are obtained via a plane-wave empirical pseudopotential approach. The empirical pseudopotentials were carefully fitted[14] to the many-body-corrected (GW) band structures,[25,26] experimental band gaps,[27,28] and LDA deformation potentials. Reference 14 gives the pseudopotentials and compares the calculated properties of bulk GaN, GaP, and GaAs to experiment

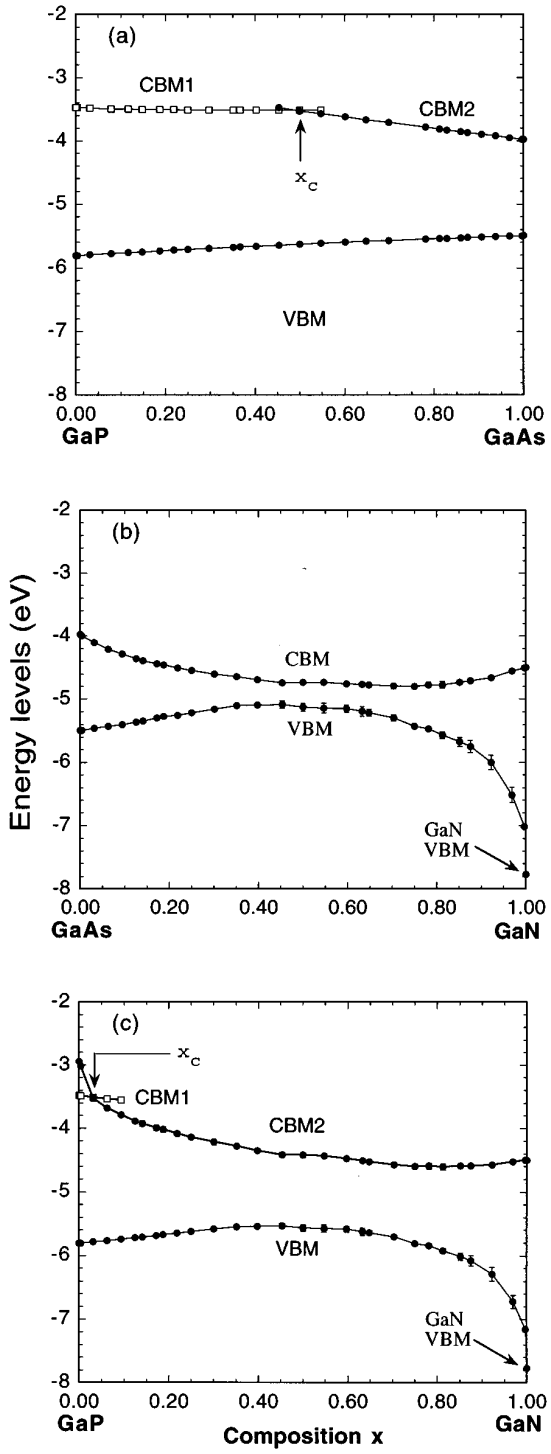

FIG. 1. Composition dependence of the near-edge energy levels of the 512-atom supercell of (a) $GaP_{1-x}As_x$, (b) $GaAs_{1-x}N_x$, and (c) $GaP_{1-x}N_x$ as obtained from atomically relaxed empirical pseudopotential calculations using Vegard's rule for the lattice constant. The valence-band energy is taken as an average over the top three crystal-field split components. Analysis of the wave functions shows that, in GaPAs and GaPN, the CBM reverts from a mostly X_{1c} character (CBM1) to another state (CBM2) that has some Γ_{1c} character. The transition point is $x_c = 0.03$ in $GaP_{1-x}N_x$ and $x_c = 0.50$ in $GaP_{1-x}As_x$. The bars denote the statistical fluctuations for different, randomly selected configurations, while the arrows emphasize the deep-gap level of GaN:As and GaN:P.

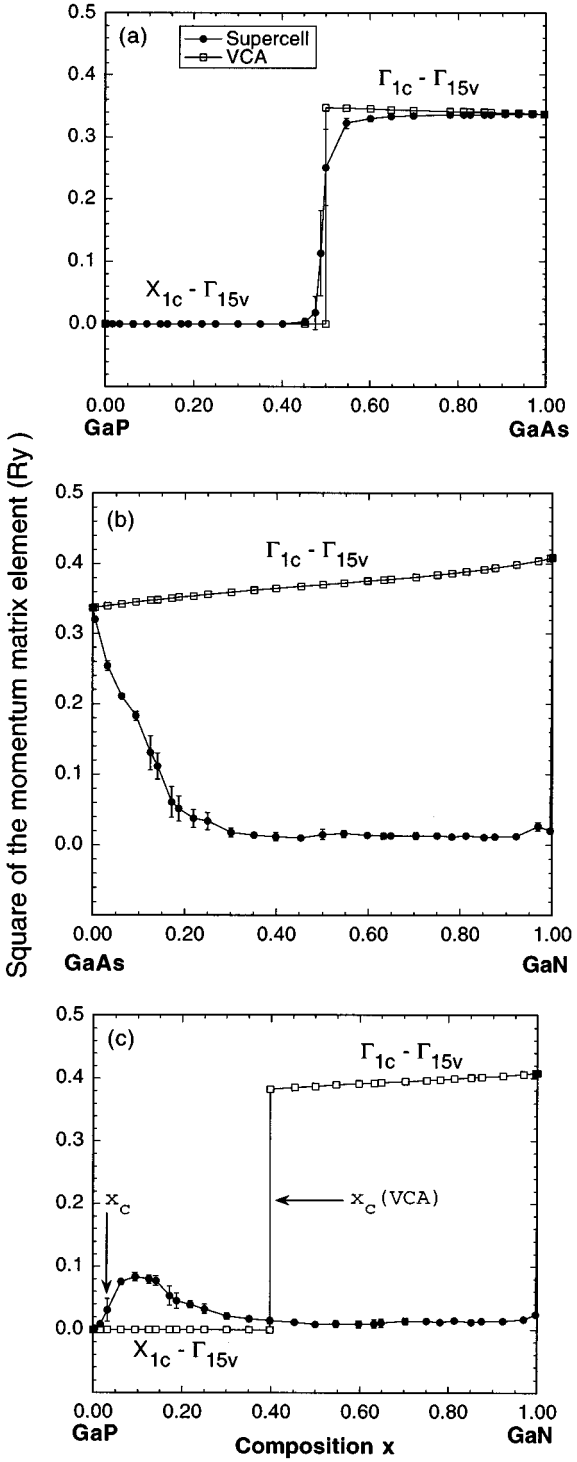

FIG. 2. Square of the momentum matrix element [Eq. (2)] for the VBM-CBM transition from the supercell (solid dots) and the unrelaxed VCA (open squares) calculations in (a) $GaP_{1-x}As_x$, (b) $GaAs_{1-x}N_x$, and (c) $GaP_{1-x}N_x$. The arrows in (c) point to the composition x_c of the X_{1c}/Γ_{1c} transition in $GaP_{1-x}N_x$. The bars denote the statistical fluctuations for different, randomly selected configurations.

as well as to other calculations. Due to the large lattice mismatch between GaAs or GaP and GaN, the pseudopotentials were fitted using a composition-dependent kinetic-energy cutoff $G_{\max}^2$ in order to keep the same number of plane waves

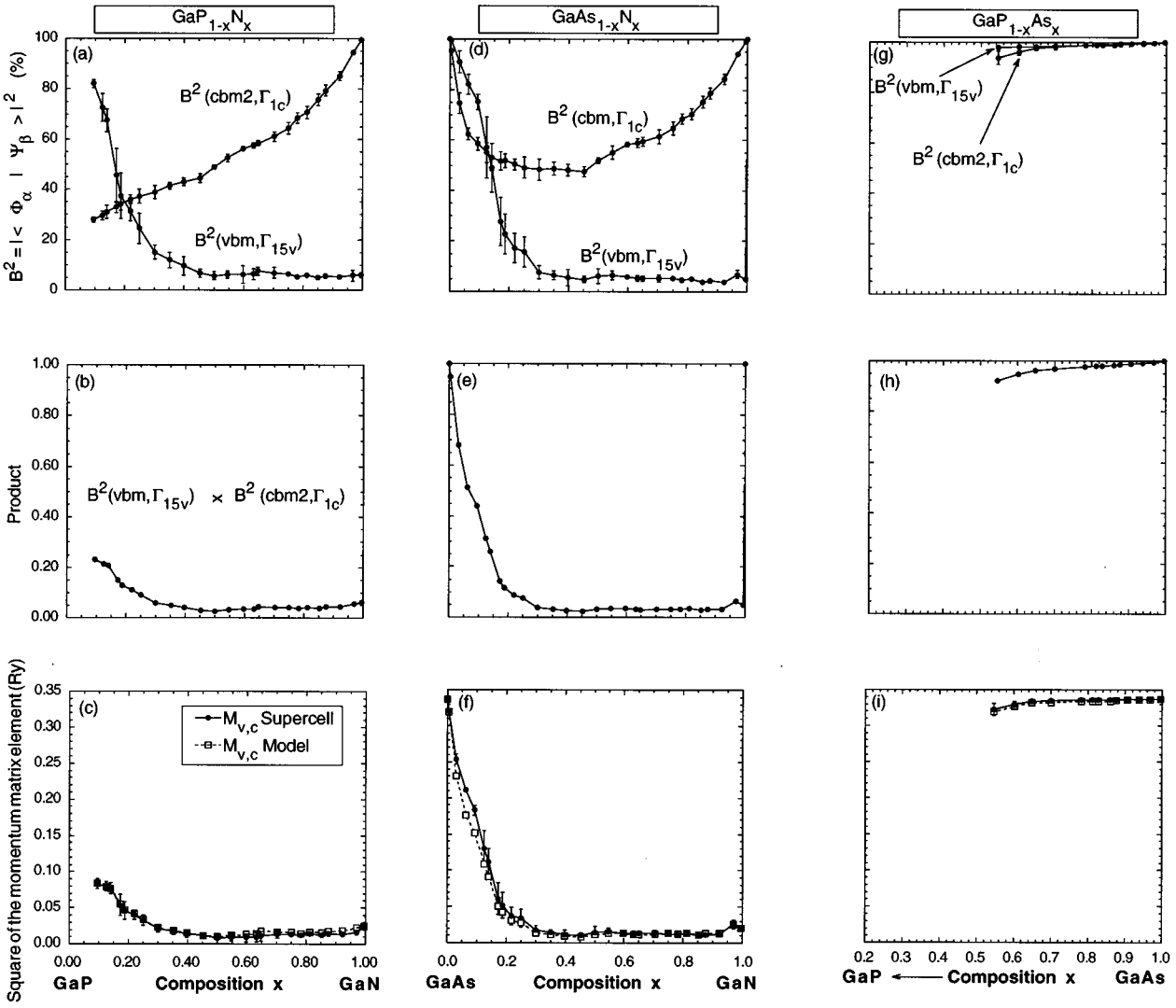

FIG. 3. (a), (d), and (g) Projection $B_{\mathrm{VBM},\Gamma_{15v}}$ of the supercell VBM wave functions onto the VCA Γ_{15v} state and $B_{\mathrm{CBM},\Gamma_{1c}}$ of the supercell CBM wave function onto the VCA Γ_{1c} state [Eq. (4)]. (b), (e), and (h) The product of projections in (a), (d), and (g). (c), (f), and (i) The product of projections times the VCA transition matrix element. This quantity (''model'') depicted in open squares is the square of the first term of Eq. (3). The squares of the momentum matrix element as computed directly in the supercell are shown as solid dots. The error bars are statistical fluctuations in configurational sampling.

per zinc-blende cell for all the compositions (i.e., volumes). This kinetic-energy cutoff $G^2_{\max}$ is 5 Ry for GaAs and GaP and 7.87 Ry for GaN, corresponding, in all cases, including our supercell calculations, to 59 plane waves at Γ per two-atom zinc-blende cell. Since we used *screened* pseudopotentials, our eigenvalues are ''absolute,'' so we can plot separately VBM and CBM energies versus composition. Indeed, superlattice calculations show that the band offsets are the difference between eigenvalues of the constituents.

To calculate near-gap energy levels of large supercells, we use the ''folded spectrum method'':[29] this is a linear-in-size $[O(N)]$ method, producing single-particle eigensolutions in a given energy window without having to obtain (and orthogonalize to) lower eigensolutions. At each composition, results are averaged over a few randomly selected configurations.

Finally, the square of the momentum matrix element is calculated in reciprocal-space from

$$M_{v,c}(\mathbf{K}) = \left|\langle \psi_v(\mathbf{K},\mathbf{r})|\mathbf{p}|\psi_c(\mathbf{K},\mathbf{r})\rangle\right|^2 = \left|\sum_{\mathbf{G}} \mathbf{G} C_v^*(\mathbf{K},\mathbf{G}) C_c(\mathbf{K},\mathbf{G})\right|^2, \quad (2)$$

where the sum runs over the vectors of the reciprocal space and $C_v(\mathbf{K},\mathbf{G})$ and $C_c(\mathbf{K},\mathbf{G})$ are the coefficients of the plane-wave expansion.

III. RESULTS

Figure 1 depicts the composition dependence of the VBM and the CBM energies in $GaP_{1-x}As_x$ [Fig. 1(a)], $GaAs_{1-x}N_x$ [Fig. 1(b)], and $GaP_{1-x}N_x$ [Fig. 1(c)]. We see significant differences in the behavior of the two kinds of alloys: The weakly interacting $GaP_{1-x}As_x$ system (Table I) has much smaller bowing compared to the strongly interacting $GaAs_{1-x}N_x$ and $GaP_{1-x}N_x$ alloys. Analysis of the corre-

sponding wave functions via Eq. (1) shows that in $GaP_{1-x}As_x$ the CBM (denoted CBM1 in Fig. 1) has mostly X_{1c} symmetry up to $x_c \simeq 0.50$, at which point it reverts to a state (denoted CBM2 in Fig. 1) that has mostly Γ_{1c} symmetry. The calculated crossover composition is in good agreement with the experimental results[30–33] of $x_c = 0.51-0.55$. For $GaP_{1-x}N_x$, we predict a crossover composition $x_c = 0.03$ between the conduction states CBM1 (mostly X_{1c} like) and CBM2 (contains a Γ_{1c} component as well as many other states). We are not aware of any direct experimental determination of the crossover composition in $GaP_{1-x}N_x$. This crossover might be difficult to detect experimentally since, unlike the case of $GaP_{1-x}As_x$, the transition in $GaP_{1-x}N_x$ is not abrupt [see Fig. 2(c)]: the ''allowed/direct'' CBM2 state is only weakly allowed, while the transition to higher-energy conduction bands may be even weaker. The significant enhancement of the PL intensity observed in $GaP_{1-x}N_x$ by Baillargeon *et al.*,[13] between $x = 0.0$ and 0.01 could be the signature of this crossover. On the other hand, there is no crossover in $GaAs_{1-x}N_x$: The CBM state contains mainly Γ_{1c} components all over the composition range.

In what follows we will focus primarily on what we will call the ''direct-gap region'' of these alloys, i.e., for all the compositions in $GaAs_{1-x}N_x$ and in the regions where the CBM is the CBM2 state in $GaP_{1-x}As_x$ and $GaP_{1-x}N_x$.

Figure 2 depicts the square of the momentum matrix element [Eq. (2)] for the VBM↔CBM transition in $GaP_{1-x}As_x$ [Fig. 2(a)], $GaAs_{1-x}N_x$ [Fig. 2(b)], and $GaP_{1-x}N_x$ [Fig. 2(c)]. For comparison with the supercell results, the square of the momentum matrix element calculated from the VCA is also given. In $GaP_{1-x}As_x$, the VCA value of $M_{v,c}$ follows the value from the supercell calculation rather well and both are nearly composition independent in the direct-gap region. This is also the case in $Ga_{1-x}Al_xAs$ alloys.[11] On the other hand, in $GaAs_{1-x}N_x$ and $GaP_{1-x}N_x$, the VCA misses both the composition dependence and the magnitude of $M_{v,c}$ as obtained in the supercell calculation.

To understand why the supercell calculations predicts a weaker and composition-dependent intensity for interband transitions in $GaAs_{1-x}N_x$ and $GaP_{1-x}N_x$ relative to $GaP_{1-x}As_x$, we use Eq. (1) to calculate the $\mathbf{K}=\mathbf{0}$ momentum matrix element for the VBM↔CBM transition in the direct-gap region of the alloy:

$$\begin{aligned}\langle \psi_{\mathrm{VBM}}|\mathbf{p}|\psi_{\mathrm{CBM}}\rangle &= \sum_{\mathbf{k},\mathbf{k}'}\sum_{j,j'} B_{\mathrm{VBM},j}(\mathbf{0},\mathbf{k})B_{\mathrm{CBM},j'}(\mathbf{0},\mathbf{k}') \\ &\quad\times\langle \phi_j(\mathbf{k})|\mathbf{p}|\phi_{j'}(\mathbf{k}')\rangle\delta_{\mathbf{k},\mathbf{k}'} \\ &= B_{\mathrm{VBM},\Gamma_{15v}}B_{\mathrm{CBM},\Gamma_{1c}}\langle \phi_{\Gamma_{15v}}|\mathbf{p}|\phi_{\Gamma_{1c}}\rangle \\ &\quad+\text{other contributions}, \end{aligned} \tag{3}$$

where

$$B_{\mathrm{VBM},\Gamma_{15v}} = \langle \psi_{\mathrm{VBM}}|\phi_{\Gamma_{15v}}\rangle,$$

$$B_{\mathrm{CBM},\Gamma_{1c}} = \langle \psi_{\mathrm{CBM}}|\phi_{\Gamma_{1c}}\rangle, \tag{4}$$

and $\langle \phi_{\Gamma_{15v}}|\mathbf{p}|\phi_{\Gamma_{1c}}\rangle$ is the momentum matrix element in the VCA (the square symbols in Fig. 2 represent the square of this element).

TABLE II. Structural and electronic properties of N impurity in GaP (GaP:N) and P impurity in GaN (GaN:P). The charges Q (see Ref. 14) are calculated using a 512-atom cell. $R_{\text{Ga-N}}$ and $R_{\text{Ga-P}}$ are the nearest-neighbor bond lengths. We found three different N-localized levels in GaP:N: (i) a level located 0.005 eV *below* the CBM of GaP, which has mainly X_{1c} character [this is the well-known shallow isolated nitrogen state of GaP:N (Refs. 34 and 35)]; (ii) a resonant level located 0.222 eV above the X_{1c} CBM of GaP, which has mainly L_{1c} character; and (iii) a resonant level discussed in the text and shown in this table, which is located 0.458 eV above the X_{1c} CBM of GaP (0.076 eV below Γ_{1c}) and has a significant Γ_{1c} character. On the other hand, GaN:P shows a deep level at 0.610 eV above the VBM.

Property	GaP and GaP:N	GaN and GaN:P
Pure host		
$Q_{\Gamma_{15v}}$ (anion)	1.86	4.16
$Q_{\Gamma_{15v}}$ (cation)	0.46	0.30
$Q_{\Gamma_{1c}}$ (anion)	3.31	4.81
$Q_{\Gamma_{1c}}$ (cation)	1.65	1.18
$R_{\text{Ga-P}}$ (Å)	2.36	
$R_{\text{Ga-N}}$ (Å)		1.95
Impurity		
$Q_{\text{impurity level}}$	1.32 (Ga) 21.72 (N) 2.10 (P)	0.84 (Ga) 205 (P) 1.9 (N)
energy level (eV)	$\epsilon_{\Gamma_{1c}} - 0.076$	$\epsilon_{\Gamma_{15v}} + 0.61$
$R_{\text{Ga-N}}$ (Å)	2.02	1.95
$R_{\text{Ga-P}}$ (Å)	2.36	2.21

Figure 3(a) shows the composition dependence of the projections $B^2_{\mathrm{VBM},\Gamma_{15v}}$ and $B^2_{\mathrm{CBM},\Gamma_{1c}}$ in $GaP_{1-x}N_x$, while Figs. 3(d) and 3(g) show analogous results for $GaAs_{1-x}N_x$ and $GaP_{1-x}As_x$, respectively. Note how strongly composition dependent these projections are in $GaP_{1-x}N_x$ and $GaAs_{1-x}N_x$ relative to the analogous results in $GaP_{1-x}As_x$. Figures 3(b), 3(e), and 3(h) show the product $B^2_{\mathrm{VBM},\Gamma_{15v}}B^2_{\mathrm{CBM},\Gamma_{1c}}$ in $GaP_{1-x}N_x$, $GaAs_{1-x}N_x$, and $GaP_{1-x}As_x$, respectively. These quantities already resemble closely the alloy intensity [Figs. 2(a)–2(c)]. This point is further demonstrated in Figs. 3(c), 3(f), and 3(i) that compare the square of the first term of Eq. (3) [The ''model,'' in square symbols in Figs. 3(c), 3(f), and 3(i)] with the directly calculated transition element of Eq. (2) [solid circles in Figs. 3(c), 3(f), and 3(i)]. The excellent agreement between the model results and the direct calculations indicates that (i) the transition intensity in the alloy is dominated by the first term in Eq. (3) and (ii) the behavior of $M_{v,c}$ in $GaAs_{1-x}N_x$ and $GaP_{1-x}N_x$ stems from the properties of the projections $B_{\mathrm{VBM},\Gamma_{15v}}$ and $B_{\mathrm{CBM},\Gamma_{1c}}$. In the following, the origin of the behavior of these projections shown in Fig. 3 is examined.

First, the projections at the impurity limit are considered. Figure 3(a) shows that, in $GaP_{1-x}N_x$, $B_{\mathrm{VBM},\Gamma_{15v}}$, decreases *discontinuously and significantly* from pure GaN ($x=1$ and $B_{\mathrm{VBM},\Gamma_{15v}}=1$) to $x=1-\epsilon$. Also, $B_{\mathrm{CBM},\Gamma_{1c}}$, decreases discontinuously and significantly from pure GaP ($x=0$ and $B_{\mathrm{CBM},\Gamma_{1c}}=1$) to $x=0+\epsilon$. These trends can be understood

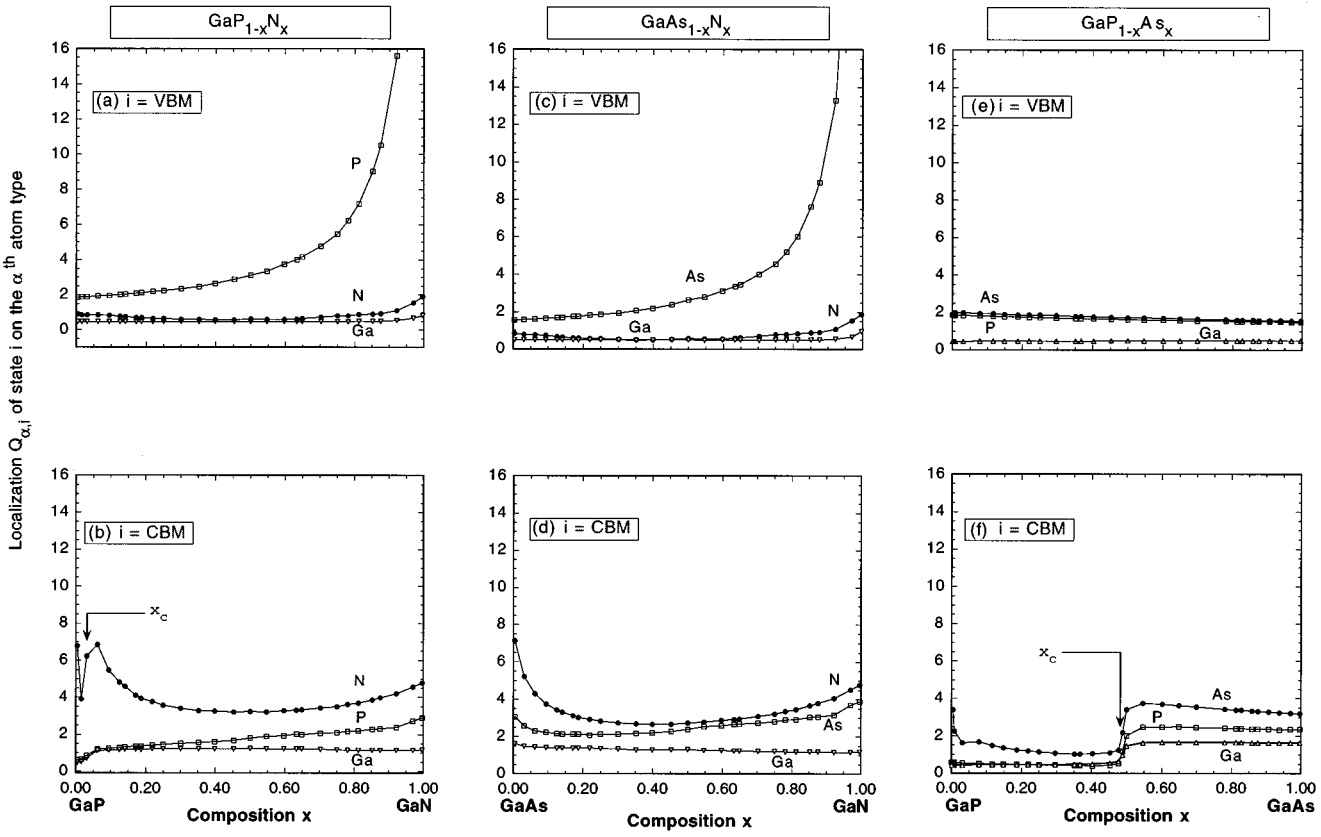

FIG. 4. Average localization parameter $Q_{\alpha,i}$ (Ref. 14) of the supercell state $i=$VBM and $i=$CBM of atoms of type $\alpha=$(As,P,N,Ga).

by considering Table II: Phosphorus-doped GaN (denoted GaN:P) is predicted to have a deep, P-localized level [located at 0.61 eV above the VBM of pure GaN (close to the experimental estimate[36] of 0.57 eV for the wurtzite structure)], while nitrogen-doped GaP (denoted GaN:P) has an N-localized level [CBM2 in Fig. 1(c)] (located at 0.076 eV below the Γ_{1c} state of pure GaP). Since these impurity states are strongly localized in the real space around the impurity atoms, their wave functions are spread in k space. Due to the wave-function normalization, the projection from the Γ_{15v} or Γ_{1c} VCA state on these impurity states is then reduced by localization. This explains why $B_{\mathrm{VBM},\Gamma_{15v}}$ is small in $GaP_{\epsilon}N_{1-\epsilon}$ and why $B_{\mathrm{CBM},\Gamma_{1c}}$ is also small in $GaP_{1-\epsilon}N_{\epsilon}$.

The charge localization parameter $Q_{\alpha,i}$ at atom α of the alloy state $\psi_{i=\mathrm{VBM}}$ or $\psi_{i=\mathrm{CBM}}$ defined in Ref. 14 and displayed in Fig. 4 shows how the VBM wave function becomes more delocalized as the P concentration increases, explaining why $B_{\mathrm{VBM},\Gamma_{15v}}$ approaches continuously its value of 100% at GaP:N. Similarly, the CBM wave function becomes more extended as the N compositions increase [Fig. 4(b)], explaining why $B_{\mathrm{CBM},\Gamma_{1c}}$ increases progressively until reaching the value of 100% at GaN:P. Since in $GaP_{1-x}N_x$ the VBM and CBM wave-function localizations occur in different composition regions (high x versus small x, respectively), the product $B^2_{\mathrm{VBM},\Gamma_{15v}}B^2_{\mathrm{CBM},\Gamma_{1c}}$ is much smaller than 1 for all compositions. This explains why the momentum matrix element of $GaP_{1-x}N_x$ is so weak, in comparison with ''normal'' alloys or with the VCA description of $GaP_{1-x}N_x$. We thus conclude that the weakness of the transition matrix element of $GaP_{1-x}N_x$ reflects wave-function localizations in different composition regions and that these localizations are due to the existences of impurity levels at the dilute impurity limits.

The situation is different in the weakly perturbed $GaP_{1-x}As_x$ system: Since there are no deep impurity levels for GaP:As and GaAs:P,[14] there is no discontinuity of the projections [Fig. 3(g)] at the dilute impurity limits and there is no localization in $GaP_{1-x}As_x$ [Figs. 4(e) and 4(f)]. The projections in this alloy (Fig. 3) are thus nearly composition independent in the direct-gap region. Consequently, the interband transition probability is large and nearly composition independent in the direct-gap region.

The situation for the $GaAs_{1-x}N_x$ system is intermediate between GaPN and GaPAs: GaN:As has a deep, As-localized impurity level located at 0.75 eV above the VBM of pure GaN,[14] while no impurity state, with Γ_{1c} or Γ_{15v} components, is found for N-doped GaAs.[14] Thus the discontinuity and the weakness of the projections at the dilute impurity limits of this alloy occur only for $B_{\mathrm{VBM},\Gamma_{15v}}$ at $x=1-\epsilon$ [Fig. 3(d)]. The product of the projections is then large for small x and very small for large N compositions where the VBM is strongly localized around the arsenic atoms [see Fig. 3(d)]. Thus this product is strongly composition dependent. We thus conclude that the composition dependence of the transition matrix element of $GaAs_{1-x}N_x$ is due to the existence of an impurity level at ''only'' one impurity limit: GaN:As.

Wave-function localizations and their ensuing effects on

the alloy could be caused by pure chemical differences between the alloyed elements (as measured, e.g., by the electronegativity difference) or by size differences. To examine which of the two effects is more important, we have selectively eliminated one: We repeated our calculations of the matrix elements in $GaP_{1-x}N_x$ and $GaAs_{1-x}N_x$ *neglecting atomic relaxations* for large x, so the difference between this unrelaxed supercell calculation and the unrelaxed VCA is purely chemical. We found that in the direct-band-gap region (i) the momentum matrix element is composition independent and nearly equal to the VCA value, (ii) the band-edge wave functions are extended with large Γ_{15v} or Γ_{1c} characters (more than 95%), and (iii) there is no gap impurity level for Ga<u>N</u>:P and Ga<u>N</u>:As. Thus we conclude that the strong wave-function localizations and the ensuing weakness of the transition intensities are mostly induced by atomic relaxations for large nitrogen compositions in $GaP_{1-x}N_x$ and $GaAs_{1-x}N_x$.

IV. SUMMARY

We find that in the GaPN alloys (i) the chemical and particularly the size differences between the two anions lead to localized impurity states in the dilute impurity limits: a P-localized deep impurity state in Ga<u>N</u>:P and an N-localized resonant state in Ga<u>P</u>:N; (ii) these states develop into a P-localized VBM in N-rich alloys [Fig. 4(a)] and to an N-localized CBM in P-rich alloys [Fig. 4(b)]; (iii) these alloy localizations lead to a small projection of the VBM on Γ_{15v} in N-rich alloys and to a small projection of the CBM on Γ_{1c} in P-rich alloys [Fig. 3(a)]; and (iv) this composition dependence of the projections, when multiplied $[B^2_{\mathrm{VBM},\Gamma_{15v}} B^2_{\mathrm{CBM},\Gamma_{1c}}$; see Fig. 3(b)], explain the weak and slightly composition-dependent VBM-CBM dipole matrix element in $GaP_{1-x}N_x$ [Fig. 3(c)]. The virtual-crystal approximation forces all anions in $GaP_{1-x}N_x$ to be chemically and, more important, structurally identical. Thus the localization and the composition dependence of the interband matrix element are not allowed in the VCA. In $GaP_{1-x}As_x$ there are no localized states in the impurity limit, so effects (ii)–(iv) do not exist and the VCA becomes a good approximation for the matrix elements. The situation for $GaAs_{1-x}N_x$ is intermediate between $GaP_{1-x}N_x$ and $GaP_{1-x}As_x$: Ga<u>N</u>:As has a deep impurity level, while Ga<u>As</u>:N has no impurity state, with Γ_{1c} or Γ_{15v} components. This leads to a strongly composition dependence of the dipole matrix element [Fig. 3(f)]: $M_{v,c}$ is large for small x and very small for large x.

We wish to emphasize that the calculations here assume a perfectly random alloy, while in reality one might expect important deviations from randomness in the form of clustering[20] or ordering. These may affect optical bowing and momentum matrix elements significantly.

ACKNOWLEDGMENTS

We wish to thank Y. Zhang for useful discussions and A. Franceschetti for use of his momentum matrix element code. This work was supported by the U.S. Department of Energy, OER-BES-DMS Grant No. DE-AC36-83-CH10093.

[1] A. Zunger, in *First Principles Statistical Mechanics of Semiconductor Alloys and Intermetallic Compounds*, Vol. 319 of *NATO Advanced Study Institute, Series B: Physics*, edited by P. Turchi and A. Gonis (Plenum, New York, 1994), pp. 361–419.

[2] S.-H. Wei, L. G. Ferreira, and A. Zunger, Phys. Rev. B **41**, 8240 (1990).

[3] A. Zunger, S.-H. Wei, L. G. Ferreira, and J. E. Bernard, Phys. Rev. Lett. **65**, 353 (1990).

[4] S.-H. Wei, L. G. Ferreira, J. E. Bernard, and A. Zunger, Phys. Rev. B **42**, 9622 (1990).

[5] S.-H. Wei and A. Zunger, Phys. Rev. B **43**, 1662 (1991).

[6] R. Magri, S. Froyen, and A. Zunger, Phys. Rev. B **44**, 7947 (1991).

[7] Z. W. Lu, S.-H. Wei, and A. Zunger, Phys. Rev. B **44**, 10 470 (1991).

[8] Z. W. Lu, S.-H. Wei, and A. Zunger, Phys. Rev. B **44**, 3387 (1991).

[9] J. L. Martins and A. Zunger, Phys. Rev. B **30**, 6217 (1984).

[10] J. C. Mikkelsen, Jr. and J. B. Boyce, Phys. Rev. Lett. **49**, 1412 (1982).

[11] B. Koiller and R. B. Capaz, Phys. Rev. Lett. **74**, 769 (1995).

[12] N. Yoshimoto, T. Matsuoka, T. Sasaki, and A. Katsui, Appl. Phys. Lett. **57**, 1031 (1990).

[13] J. N. Baillargeon, K. Y. Cheng, G. E. Hofler, P. J. Pearah, and K. C. Hsieh, Appl. Phys. Lett. **60**, 2540 (1992).

[14] L. Bellaiche, S.-H. Wei, and A. Zunger, Phys. Rev. B **54**, 17 568 (1996).

[15] S.-H. Wei and A. Zunger, Phys. Rev. Lett. **76**, 664 (1996).

[16] J. C. Phillips, *Bonds and Bands in Semiconductors* (Academic, New York, 1973), p. 54.

[17] D. M. Ceperley and B. J. Alder, Phys. Rev. Lett. **45**, 566 (1980).

[18] J. Perdew and A. Zunger, Phys. Rev. B **23**, 5048 (1981).

[19] R. G. Dandrea and A. Zunger, Appl. Phys. Lett. **57**, 1031 (1990).

[20] K. Mader and A. Zunger, Phys. Rev. B **51**, 10 462 (1995).

[21] P. N. Keating, Phys. Rev. **145**, 637 (1966).

[22] R. M. Martin, Phys. Rev. B **1**, 4005 (1970).

[23] J. Neugebauer and C. G. Van de Walle, Phys. Rev. B **51**, 10 568 (1995).

[24] K. Kim, W. R. L. Lambrecht, and B. Segall, Phys. Rev. B **53**, 16 310 (1996).

[25] A. Rubio, J. L. Corkhill, M. L. Cohen, E. Shirley, and S. Louie, Phys. Rev. B **48**, 11 810 (1993).

[26] M. Palummo, L. Reining, R. W. Godby, C. M. Bertoni, and N. Bornsen, Europhys. Lett. **26**, 607 (1994).

[27] *Properties of Group III Nitrides*, edited by J. H. Edgar, Emis Data Reviews Series No. 11 (Inspec, London, 1994).

[28] D. S. Kyser and V. Rehn, Phys. Rev. Lett. **40**, 1038 (1978).

[29] L.-W. Wang and A. Zunger, J. Chem. Phys. **100**, 2394 (1994).

[30] M. G. Craford, R. W. Shaw, A. H. Herzog, and W. O. Groves, J. Appl. Phys. **43**, 4075 (1972).

[31] A. Onton and L. M. Foster, J. Appl. Phys. **43**, 5084 (1972).
[32] R. J. Nelson, N. Holonyak, and W. O. Groves, Phys. Rev. B **13**, 5415 (1976).
[33] H. Mathieu, P. Merle, and E. L. Ameziane, Phys. Rev. B **15**, 2048 (1977).
[34] W. Czaja, Festkoerperprobleme **11**, 65 (1971).
[35] Y. Zhang, W. Ge, M. D. Sturge, J. Zheng, and B. Wu, Phys. Rev. B **47**, 6330 (1993).
[36] J. I. Pankove and J. A. Hutchby, J. Appl. Phys. **47**, 5387 (1976).